West-East High Speed Flow Field Conference
19-22, November 2007
Moscow, Russia

METRIC-BASED MESH ADAPTATION IN ALE SIMULATION

Konstantin Lipnikov[1] **Yuri Vassilevski**[2]

[1] *Los Alamos National Laboratory, Theoretical Division, MS B284, Los Alamos, NM, 87545, USA.*
lipnikov@lanl.gov
[2] *Institute of Numerical Mathematics RAS, 8, Gubkina, 119333, Moscow, Russia.*
vasilevs@dodo.inm.ras.ru

Key words: ALE simulation, mesh adaptation, metric recovery.

Abstract. We present a new moving mesh method for arbitrary Lagrangian-Eulerian simulations. The mesh motion is reduced to generation of a mesh which is quasi-uniform in a space metric induced by the solution gradient. The new method generates meshes which satisfy practical requirements such as mesh smoothness and bounded variation of mesh size. Two numerical examples demonstrate basic features of the method and its applicability to gas dynamic problems.

1. INTRODUCTION

The arbitrary Lagrangian-Eulerian (ALE) simulation combines the best properties of Eulerian and Lagrangian simulations. In most ALE methods, the computational mesh remains shape-regular (as in Eulerian methods) during the whole simulation and at the same time it follows the fluid flow (as in Lagrangian methods). When dynamics of fluid flow does not match error dynamics, the mesh motion should be driven by the error dynamics, and this is the motivation for using ALE methods.[1,11,13] In this article, we present a new method for the mesh motion based on error dynamics.

The ALE cycle consists of three major steps: an explicit Lagrangian step, a mesh motion step, and a remapping step.[1,8,9,11,13] Since each step contributes to the total error, the *ideal* mesh motion method should target this total error. Analysis of the total error for smooth solutions implies that the optimal mesh should be quasi-uniform in a metric induced by the solution gradient. We extrapolate this result to problems with shocks and base the space metric on the discrete gradient. We propose to use the reaction-diffusion equation to smooth the discrete gradient to avoid unphysical mesh clustering around shocks. We also *lift* the metric by adding a small positive constant to it in order to avoid creation of huge cells in regions where the gradient is close to zero.

The mesh motion methods based on monitor function also use the solution gradient.[2,5,13] However, there are a few significant differences with the approach developed in this article. First, we perform the metric smoothing in the physical space.

For smooth solutions this results in the rigorous control of the error. Second, we use the weak formulation of the discrete gradient instead of its explicit form. This technique smears numerical instabilities related to finite differencing.

We also mention methods which use different geometric principles to relax the Lagrangian mesh.[4,7,9]

The article is organized as follows. In Section 2 we recall basics of the ALE simulation, the objective of the mesh motion step, and its connection with a metric-based adaptation method. In Section 3 we introduce and analyze new approach to automated metric recovery. In Section 4 we present the new mesh motion method. Numerical results for two 1D model problems are discussed in Section 5. In Appendix we motivate briefly the use of metric-based adaptation in ALE framework for the case of smooth solution.

2. BASICS OF ARBITRARY LAGRANGIAN-EULERIAN SIMULATION

Let the superscript n specify the time step for all grid functions. At time $t = t^n$, the mesh $\mathbf{x}^n$ on $[a, b]$ is represented by the ordered set of nodes:

$$a = x_0^n < x_1^n < \cdots < x_{M+1}^n = b. \tag{1}$$

Let $h_{i+1/2}^n = x_{i+1}^n - x_i^n$ denote the length of the mesh interval $[x_i,\, x_{i+1}]$ which we shall refer to as the cell.

Let $u(x,t)$ be the solution of a conservation law

$$\frac{\partial u}{\partial t} + \frac{\partial (F(u))}{\partial x} = 0 \tag{2}$$

subject to appropriate initial and boundary conditions.

Let $\bar{\mathbf{u}}^n$ be an approximation of $u(x,t)$ represented by cell-centered values $\bar{u}_{i+1/2}^n$. Hereafter, $\bar{\mathbf{u}}^n$ denotes either a vector of cell-centered values or a piecewise constant function over $[a,\, b]$. The value $\bar{u}_{i+1/2}^n$ approximates the exact mean value of $u(x,t)$ on interval $[x_i^n, x_{i+1}^n]$ at time t^n:

$$\bar{u}_{i+1/2}^n \approx \bar{u}([x_i^n, x_{i+1}^n], t^n) \equiv \frac{1}{h_{i+1/2}^n} \int_{x_i^n}^{x_{i+1}^n} u(x, t^n) dx.$$

The explicit Lagrangian step can be written in an operator form

$$\bar{\mathbf{u}}^{n+1} = \mathcal{L}^n(\bar{\mathbf{u}}^n) \tag{3}$$

where $\mathcal{L}^n$ is one of the popular time integration methods for (2).

The idea of the mesh motion step is to replace the mesh $\mathbf{x}^n$ with a new mesh $\tilde{\mathbf{x}}^n$ to minimize the error after one step of the ALE method. This error consists of three pieces: the remapping error, the time integration error and the space discretization error. When $\tilde{\mathbf{x}}^n = \mathbf{x}^n$, the remapping error is zero; however, the two other errors may be too large. Thus, the objective of the *ideal* mesh motion step is to find a mesh which balances these three errors such that the overall error is minimized. Let $\overline{\tilde{\mathbf{u}}}^n$ denote the solution remapped on mesh $\tilde{\mathbf{x}}^n$. Then, the optimal mesh is a solution of the following minimization problem:

$$\tilde{\mathbf{x}}_{opt}^n = \arg \min_{\tilde{x}_1^n \ldots \tilde{x}_M^n} \|u(x, t^{n+1}) - \mathcal{L}^n(\overline{\tilde{\mathbf{u}}}^n)\|_{L_1([a,b])}. \tag{4}$$

The L_1-norm of the error is conventional for gas dynamic models featuring strong shocks.

The exact solution of (4) is usually not practical. In practice, the mesh $\tilde{\mathbf{x}}^n$ must satisfy the following two conditions.

(C1) Let $\mathcal{H}$ be the ratio of maximal and minimal cell sizes in mesh $\tilde{\mathbf{x}}^n$,

$$\mathcal{H} = \max_{0 \leqslant i \leqslant M} \tilde{h}^n_{i+1/2} \Big/ \min_{0 \leqslant i \leqslant M} \tilde{h}^n_{i+1/2}.$$

We assume that there exists a positive (user-given) constant $\mathcal{H}_*$ such that

$$\mathcal{H} \leqslant \mathcal{H}_*. \tag{5}$$

(C2) We assume that each node of $\tilde{\mathbf{x}}^n$ deviates from the similar node of $\mathbf{x}^n$ by less than the local mesh size.

Condition **(C1)** controls the minimal mesh size and therefore the time step in the explicit Lagrangian step. It limits resolution of strong shocks and does not allow creation of large cells in regions where solution is constant. This condition is a relaxed form of the mesh quasi-uniformity condition — $\mathcal{H}_*$ may be large enough. Condition **(C2)** allows to use conservative high-order remapping methods[10] in higher-dimensions.

For a given mesh $\mathbf{x}^n$, conditions **(C1)** and **(C2)** form a closed set $\mathcal{F}(\mathbf{x}^n)$ of admissible meshes. We reformulate the optimization problem as follows:

$$\tilde{\mathbf{x}}^n_{opt} = \arg \min_{\{\tilde{x}^n_1 \ldots \tilde{x}^n_M\} \in \mathcal{F}(\mathbf{x}^n)} \|u(x, t^{n+1}) - \mathcal{L}^n(\overline{\tilde{\mathbf{u}}}^n)\|_{L_1([a,b])}. \tag{6}$$

The complete analysis of problem (6) can be done for smooth solutions[12] such that $u'(x) > 0$. In this case, the approximate solution of (6) is reduced to generation of a mesh which is quasi-uniform in metric

$$\mathcal{M}(x) = \sqrt{|u'(x)|}. \tag{7}$$

A sketch of the analysis is given in the appendix. We extrapolate this result to problems with shocks and modify it for the case when the gradient is zero in some parts of the computational domain.

3. METRIC RECOVERY, SMOOTHING AND LIFTING

In applications, the metric (7) is not known. Therefore, the solution gradient $|u'|$ has to be replaced by the discrete gradient $|u'_h|$ which is not an accurate approximation of $|u'|$, especially for problems with shocks. Moreover, the recovered discrete gradient is usually a non-smooth function and may be even equal to zero in some parts of the computational domain. This explains why it is never used directly for building a space metric.

Different monitor functions using *ad hoc* modifications of the discrete gradient can be found in the literature.[2,5] Most efficient modifications use the Laplacian smoother defined in a reference (logical) space. We propose (a) to apply smoothing in *physical space* and (b) to define the smoother via the reaction-diffusion equation

(9) with a mesh dependent diffusion coefficient. To satisfy condition **(C1)**, we add to the metric a rigorously defined constant. We call this metric modification as *metric lifting*. The metric $\mathcal{M}$ built below is induced by a continuous function $|v|$ such that

- the discrepancy $|v| - |u'|$ is small for a smooth function u with $u' \neq 0$ on $[a, b]$;
- rough features of $|u'_h|$ are smeared out;
- variations of $|v|$ on $[a, b]$ are limited, i.e. $\max\limits_{x\in[a,b]} |v(x)| / \min\limits_{x\in[a,b]} |v(x)| \leqslant \mathcal{H}_*$.

Let $u_h(x)$ be a piecewise constant function defined on a mesh $\mathbf{x}$ and $u'(a)$ and $u'(b)$ be known one sided derivatives of $u(x)$ at points a and b, respectively. Let V^h be the finite element space of continuous piecewise linear on $\mathbf{x}$ functions and V_0^h be its subspace of functions vanishing at points a and b. Consider the following finite element problem: Find $v_h \in V^h$ such that $v_h(a) = u'(a)$, $v_h(b) = u'(b)$, and

$$\int_a^b \left(v_h w_h + \varepsilon(x) \frac{\partial v_h}{\partial x} \frac{\partial w_h}{\partial x} \right) dx = - \int_a^b u_h \frac{\partial w_h}{\partial x} dx \qquad \forall w_h \in V_0^h, \tag{8}$$

where $\varepsilon(x)$ is a piecewise constant function:

$$\varepsilon(x) = h_{i+1/2}^2, \qquad x \in (x_i, x_{i+1}).$$

The problem (8) defines implicitly a smoothing operator S for the first derivative of u_h. Note that that first derivative of u_h is posed in a weak sense to avoid numerical instabilities in recovering u'_h. The matrix of the discrete system appearing from (8) is not stiff, since its properties are close to that of the finite element mass matrix in space V^h. Therefore, the PCG method with the Jacobi preconditioner applied to the solution of (8) converges fast. Equation (8) is the finite element discretization of the reaction-diffusion equation

$$-(\varepsilon(x)v'(x))' + v(x) = u'(x), \quad x \in (a, b), \quad v(a) = u'(a), \quad v(b) = u'(b). \tag{9}$$

When u' is a smooth function, the solution v approximates u' because of the small value of the diffusion term. When u' is a non-smooth function, the diffusion term plays an important role in smoothing the solution v. This is illustrated in Fig.1.

The finite element framework allows us to differentiate and smooth piecewise constant data u_h on non-uniform meshes. Moreover, it is possible to estimate the smoothing effect of the operator S. In view of a limited change of the mesh steps in mesh $\mathbf{x}$ (due to condition **(C1)**), there exist constants c_h, C_h such that $c_h h \leqslant h_{i+1/2} \leqslant C_h h$, and we can apply the result from.[3] Fix a small integer K and consider the problem: find $g_h \in V_h$, such that $g_h(a) = 0$, $g_h(b) = 1$ and

$$\int_a^b \left(g_h w_h + h^2 \frac{\partial g_h}{\partial x} \frac{\partial w_h}{\partial x} \right) dx = 0 \qquad \forall w_h \in V_0^h. \tag{10}$$

Then there exist constants c and γ independent of M such that

$$\sum_{i=0}^{M-K} (g_h(x_i))^2 \leqslant c e^{-\gamma K}.$$

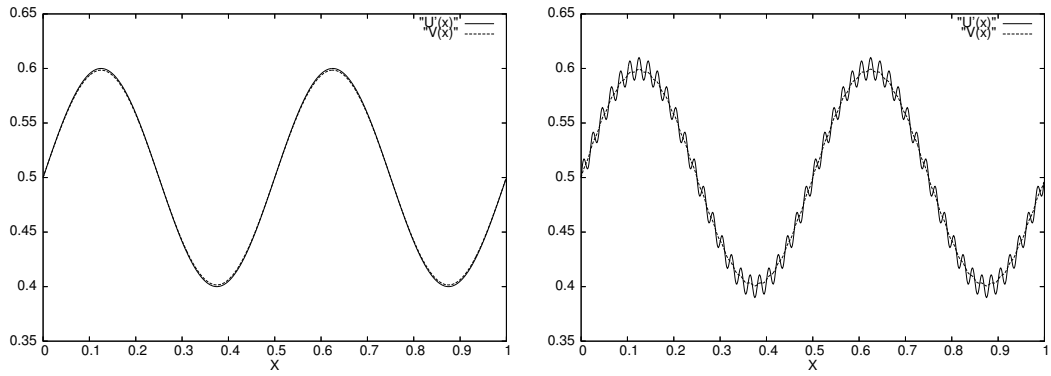

Figure 1: The solution $v(x)$ of the reaction diffusion problem for smooth (left) and non-smooth (right) function $u'(x)$, $\varepsilon = 10^{-4}$.

This inequality may be used to estimate the decay rate for the discrete Green function $G^j \in V_0^h$ associated with the j-th mesh node:

$$\int_a^b \left(G^j w_h + \varepsilon(x) \frac{\partial G^j}{\partial x} \frac{\partial w_h}{\partial x} \right) dx = w_h(x_j) \qquad \forall w_h \in V_0^h. \tag{11}$$

Thus, we have a similar estimate for $G_i^j \equiv G^j(x_i)$:

$$\sum_{i:|i-j|>K} (G_i^j)^2 \leqslant c e^{-\gamma K}. \tag{12}$$

Let us consider for simplicity the homogeneous Dirichlet boundary conditions, i.e. $v(a) = u'(a) = 0$ and $v(b) = u'(b) = 0$. The nodal value $v_h(x_i)$ of the solution to (8) may be represented as a series

$$v_h(x_i) = \sum_{1 \leqslant j \leqslant M} G_i^j U_j, \tag{13}$$

where U_j is the finite difference approximation of u' at point x_j. Formulas (12) and (13) imply that $v_h(x_i)$ is affected only by U_js in a small vicinity of x_i. Therefore, the smoothing operator S preserves the main features of u'.

Although $|v_h(x)|$ is a non-negative function, it may be close to zero for some values of x. Moreover, even if this is not the case, variation of $|v_h|$ on $[a, b]$ may be excessive. In order to guarantee strict positivity of $v_h(x)$ and to satisfy condition (5) imposed on the mesh, we modify the right hand side of equation (9) by substituting $u'(x)$ for

$$u'(x) + \max \left\{ 0, \frac{\max\limits_x u'(x) - \mathcal{H}_*^2 \min\limits_x u'(x)}{\mathcal{H}_*^2 - 1} \right\}. \tag{14}$$

To compute the lifting constant, we approximate $u'(x)$ with finite differences. The impact of the metric lifting on the interpolation error is as follows: if the lifting constant does not exceed $\|\sqrt{u'}\|^2_{L_1([a,b])}/(b-a)^2$, then the amplification of the norm of the interpolation error is bounded.[12]

Hereafter, $\mathcal{M}$ denotes the continuous metric induced by the finite element solution v_h of (8) with the right hand side modified as in the continuum case (14), i.e.

$$\mathcal{M}(x) = \sqrt{|v_h(x)|}. \tag{15}$$

4. MESH MOTION METHOD

The mesh size of the $\mathcal{M}$-uniform mesh $\mathbf{x}$ with $M+2$ nodes is computed as follows:

$$h_{\mathcal{M},i+1/2} = \frac{1}{M+1} \int_a^b \sqrt{\mathcal{M}(x)}\, dx \equiv C_{\mathcal{M}}, \qquad i = 0, \ldots, M. \tag{16}$$

We suggest a simple approach for generating a $\mathcal{M}$-quasi-uniform mesh. Starting with an arbitrary mesh with $M+2$ nodes, we compute the integral in (16) and move the mesh nodes to equidistribute $h_{\mathcal{M},i+1/2}$. A new position for the mesh node is defined in such a way to increase the *mesh quality* $Q_{\mathcal{M}}(\mathbf{x})$:

$$Q_{\mathcal{M}}(\mathbf{x}) = \min_{0 \leqslant i \leqslant M} F(z_{i+1/2}),$$

where

$$F(z) = z^3(2-z)^3, \qquad z_{i+1/2} = \min\left\{ \frac{h_{\mathcal{M},i+1/2}}{C_{\mathcal{M}}},\ \frac{C_{\mathcal{M}}}{h_{\mathcal{M},i+1/2}} \right\}.$$

Quality of the $\mathcal{M}$-uniform mesh with $M+2$ nodes equals to 1. For all other meshes, the mesh quality is strictly less than 1.

For a given mesh $\mathbf{x}$, we loop over M interior nodes that are ordered by increasing of their qualities (the quality of a mesh node is defined as the minimal quality of its neighboring elements). On each step of the loop only one node is repositioned to maximize its quality. If the required mesh quality is not reached after this loop, we reorder the mesh nodes and repeat the loop. The algorithm is terminated when $Q(\mathbf{x})$ approaches 1 (for instance, when $Q(\mathbf{x}) > Q_0$, where $Q_0 = 0.9 - 0.999$). Our experiments show robust convergence of the algorithm. We shall use this technique as the black-box ingredient of our basic mesh adaptation algorithm:

Basic mesh adaptation

1. Compute the discrete solution $\bar{\mathbf{u}}^n$ and associated mesh $\mathbf{x}^n$.
2. Recover the metric $\mathcal{M}$ from $\bar{\mathbf{u}}^n$ using (8) and (15).
3. Generate mesh $\tilde{\mathbf{x}}^n$ such that $Q_{\mathcal{M}}(\tilde{\mathbf{x}}^n) > Q_0$.

The basic mesh adaptation requires single evaluation of $\bar{\mathbf{u}}^n$. The number of loops depends on Q_0 and the quality of the initial mesh and may vary between a few tens to a few hundreds.

If the initial mesh $\mathbf{x}^n$ is far from the $\mathcal{M}$-uniform mesh, the approximation of $u'(x)$ in the right-hand side of (8) may be inadequate. In order to fix this problem, we suggest the full mesh adaptation:

Full mesh adaptation

1. Compute the discrete solution $\bar{\mathbf{u}}^n$ on mesh $\mathbf{x}^n$.

2. Recover the metric $\mathcal{M}$ from $\bar{\mathbf{u}}^n$ using (8) and (15).
3. If $Q_{\mathcal{M}}(\mathbf{x}^n) > Q_0$ then set $\tilde{\mathbf{x}}^n = \mathbf{x}^n$ and stop.
4. Otherwise, generate a new mesh $\mathbf{x}^n$ such that $Q_{\mathcal{M}}(\mathbf{x}^n) > Q_0$ and go to 1.

The full mesh adaptation requires a few evaluations of $\bar{\mathbf{u}}^n$ on different meshes (the remapping method can be used for this purpose). In general, the method of full mesh adaptation is too costly; therefore, it is not practical. Later, we use it only for comparison purpose.

A remarkable feature of the method of full mesh adaptation is that trajectories of mesh nodes are rather smooth in time provided that Q_0 is close to 1 and the analytic solution is smooth. The method of basic mesh adaptation may result in non-smooth trajectories of the mesh nodes (see Fig. 2). However, the L_1-norm of the error is not sensitive to this non-smoothness, at least for the examples considered in the next section.

The method of basic mesh adaptation may be modified to reduce further its computational cost. Since the speed of the error propagation is small in the explicit method, the quality of the mesh after each Lagrangian step is sufficiently big. Thus, at each time step we may limit the number of loops by a small integer L_{loop} ($L_{loop} = \max(10, (M+1)/10)$ in our experiments). This modification may have a smoothing effect onto the trajectories of mesh nodes, although the mesh quality is no longer close to 1 and varies between 0.3 and 0.9 indicating that the resulting mesh remains $\mathcal{M}$-quasi-uniform. We shall refer to this algorithm as the method of *incomplete* mesh adaptation.

5. NUMERICAL RESULTS

The lifting constant defined in (14) will allow us to build adaptive meshes satisfying (5). In all experiments the metric $\mathcal{M}$ is computed using (8) and (15).

5.1. Linear advection problem

We consider the following linear advection problem. Given a small $\delta > 0$, we define the function u_0 by

$$u_0(x) = \begin{cases} 0, & x \leqslant -\delta, \\ \xi(x), & -\delta < x < \delta, \\ 1, & \delta \leqslant x, \end{cases}$$

where $\xi(x)$ is the cubic cut-off function with zero first derivatives and zero values at points $x = \pm\delta$. The function $u(x,t) = u_0(x + 0.4 - t)$, $t \in [0, 0.2]$ mimics the shock propagation from 0.4 to 0.6 with constant speed 1. In order to comply with the explicit simulation limitations, we restrict the time step by $CFL = 1$.

Fig. 2 shows trajectories of interior nodes for the mesh consisting of 50 cells and methods of full and basic mesh adaptations. The initial mesh at time $t = 0$ is the same for both methods. The chosen value for the parameter $\mathcal{H}_* = 10$ does not allow to put a lot of mesh points on the strong shock ($\delta = 10^{-3}$) which makes the adaptation problem non-trivial. One can observe smooth and non-smooth trajectories of the mesh nodes for the first and the second methods, respectively. Table 1 demonstrates that (a) the mean error is reciprocal to M and $\mathcal{H}_*$, (b) the

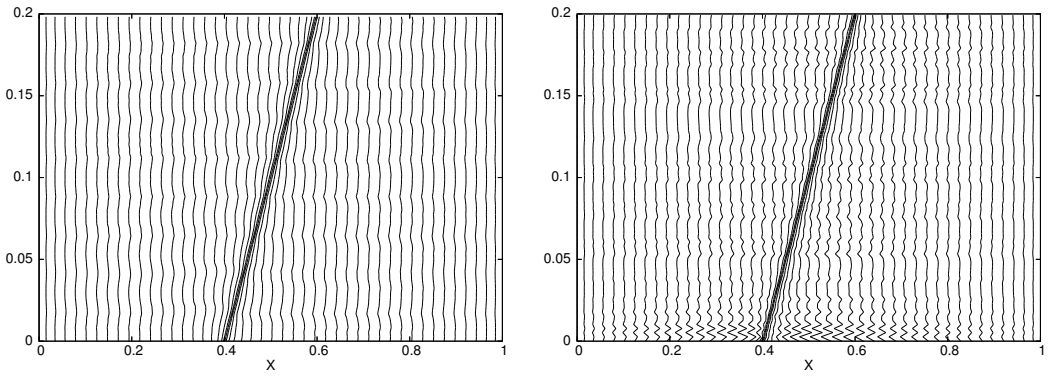

Figure 2: Linear advection problem: the method of full mesh adaptation (left) versus the method of basic mesh adaptation (right); $M = 49$, $\mathcal{H}_* = 10$, $\delta = 10^{-3}$, and $Q_0 = 0.999$.

larger M, the smaller relative deviations from the mean error, and (c) the error is the same in both methods.

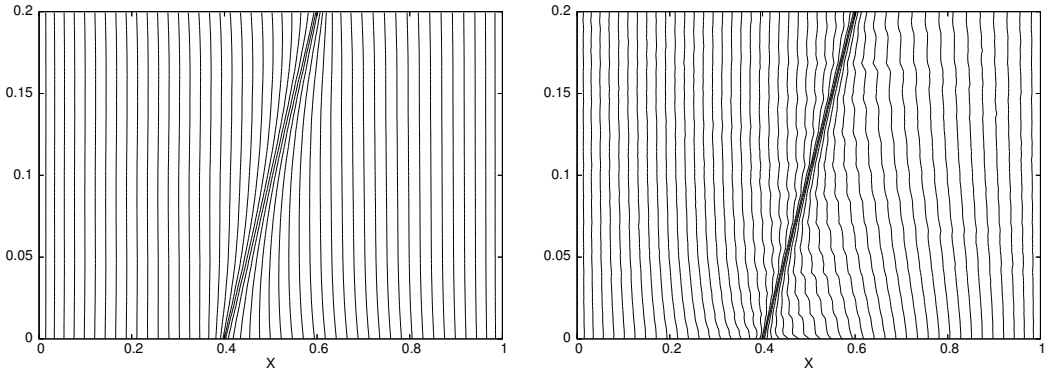

Figure 3: Linear advection problem: smoothed trajectories of mesh nodes in the method of basic mesh adaptation (left) versus trajectories of the mesh nodes in the method of incomplete mesh adaptation with $L_{loop} = 10$ (right); $M = 49$, $\mathcal{H}_* = 10$, $\delta = 10^{-3}$, and $Q_0 = 0.999$.

We did not observe any considerable negative impact of non-smoothness of the mesh trajectories on neither the L_1-norm of the error nor the error due to the remapping method, when oscillations were below 20-40% of the local mesh size. The same conclusions hold for the ALE simulation on precomputed smooth trajectories shown on the left picture in Fig. 3. The trajectories of the mesh nodes shown on the left picture in Fig. 2 are smoothed by the reaction-diffusion operator (9) posed in the time domain $(0, 0.2)$ using the piecewise constant function $\epsilon(t) = (\Delta t^{n+1})^2$ for $t \in (t^n, t^{n+1})$. The smoothing operator S is applied independently to each trajectory. Note that time-smoothing of mesh trajectories produces less condensed meshes around the shock.

Right picture in Fig. 3 shows trajectories of mesh nodes in the method of incomplete mesh adaptation with $L_{loop} = 10$. Table 1 demonstrates that the mean error increases by at most 6% although the maximum deviation from the mean value may be substantial.

Table 1: Linear advection problem: mean L_1-norm of error and the maximal deviation from the mean error (in curved brackets) for three mesh adaptation methods; $Q_0 = 0.999$, $\delta = 10^{-3}$, and $L_{loop} = \max\{10, (M+1)/10\}$.

$\mathcal{H}_*$ \ $M+1$	50	100	200
Full mesh adaptation			
10	7.4e-4 (1.4e-4)	3.2e-4 (0.4e-4)	1.5e-4 (0.3e-5)
20	3.6e-4 (0.4e-4)	1.6e-4 (0.4e-5)	8.0e-5 (1.8e-6)
40	1.9e-4 (0.3e-5)	8.7e-5 (1.5e-6)	4.2e-5 (0.5e-6)
Basic mesh adaptation			
10	7.0e-4 (2.0e-4)	3.1e-4 (0.2e-4)	1.5e-4 (5.0e-6)
20	3.5e-4 (0.4e-4)	1.6e-4 (0.6e-5)	8.0e-5 (2.7e-6)
40	1.8e-4 (0.1e-4)	8.6e-5 (1.4e-6)	4.2e-5 (0.5e-6)
Incomplete mesh adaptation			
10	7.0e-4 (2.0e-4)	3.1e-4 (0.2e-4)	1.5e-4 (6.0e-6)
20	3.6e-4 (0.5e-4)	1.6e-4 (1.3e-5)	8.0e-5 (3.7e-6)
40	1.9e-4 (0.2e-4)	9.3e-5 (7.0e-6)	4.6e-5 (2.5e-6)

5.2 Sod shock tube problem

Let us consider the system of 1D gas dynamics equations written in the Lagrangian form:

$$\begin{aligned} \frac{1}{\rho}\frac{d\rho}{dt} + \frac{\partial u}{\partial x} &= 0, \\ \rho\frac{du}{dt} + \frac{\partial p}{\partial x} &= 0, \\ \rho\frac{d\epsilon}{dt} + p\frac{\partial u}{\partial x} &= 0, \end{aligned} \tag{17}$$

where ρ is the density, u is the velocity, ϵ is the specific internal energy, and p is the pressure. The pressure is computed from the equation of state, $p = (\gamma - 1)\rho\epsilon$, where γ is the ratio of specific heats. The system (17) is closed by imposing some initial conditions and boundary conditions for either the velocity or pressure. The system is solved using the second-order predictor-corrector method.[11]

The Sod shock tube problem consists of two regions of gas with $\gamma = 1.4$ initially separated by a membrane at $x = 0.5$. The gas to the left of the membrane is more dense ($\rho_L = 1$ and $\rho_R = 0.125$) and at a higher pressure ($p_L = 1$ and $p_R = 0.1$) compared to the one on the right. We impose the reflecting boundary conditions at $x = 0$ and $x = 1$. The final time is $t = 1$ so that we can study the interaction of waves generated after removing the membrane. To compute errors we use the Lagrangian solution obtained on a fine mesh with 10^5 cells.

In all experiments the initial mesh at time $t = 0$ is adapted to the discontinuity in the density profile using the method of full mesh adaptation. The method of incomplete mesh adaptation is used for $t > 0$. Time step in numerical simulations is restricted by $CFL = 0.7$. The results of numerical experiments are shown in Fig. 4 and Table 2. The trajectories of the mesh nodes indicate clearly interaction of the reflected shock wave with the contact discontinuity. In particular, the change in the solution profile at time $t \approx 0.4$ induces the strong motion of the mesh which is

even more obvious for bigger L_{loop}. The same phenomena is observed in other mesh motion methods.[6] Since the time step remains small, the local motion of the mesh nodes is still within one mesh cell.

In the pure Lagrangian simulation the shock wave is not well resolved after $t > 0.4$ (see Fig. 4). As the result, the Lagrangian solution is about 4 times less accurate than the solution on the adapted mesh with the same number of nodes.

Since the metric $\mathcal{M}$ is chosen to minimize the error in the density profile, the error of the other physical functions may demonstrate non-optimal rate of reduction. Table 2 shows that the first-order convergence rate is not observed for all unknowns. In general, the metric may be build using the sum of weighted errors in primary variables.[6] Increasing of $\mathcal{H}_*$ results in smaller errors due to better resolution of material discontinuities and shock waves. On the other hand, the simulation requires more time steps due to the CFL restriction.

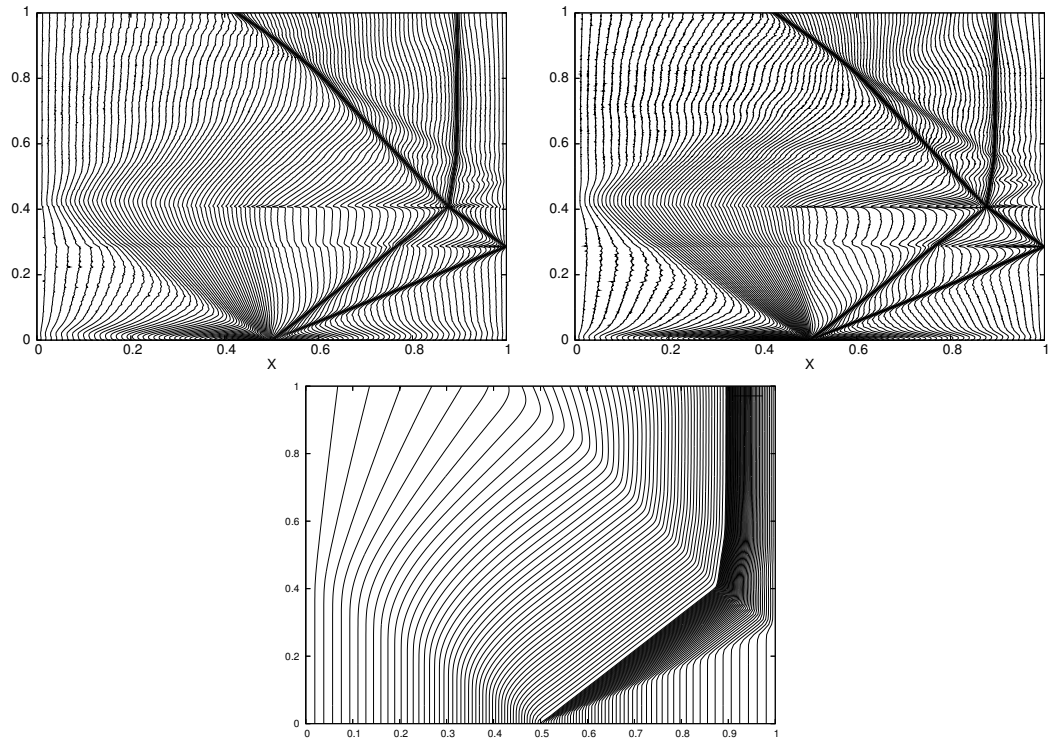

Figure 4: Trajectories of mesh points for the method of incomplete mesh adaptation with $L_{loop} = 10$ for the Sod shock tube problem; $M = 99$, $Q_0 = 0.9$. The pictures correspond to $\mathcal{H}_* = 10$ (top-left) and $\mathcal{H}_* = 20$ (top-right). The bottom picture shows trajectories of mesh points for the Lagrangian simulation.

6. CONCLUSION

We developed and studied the new moving mesh method. The existence of mathematical motivation separates our method from a large group of other moving mesh methods based on a metric or a monitor function. Most of the analysis can be extended to higher dimensions.

Table 2: Sod shock tube problem: L_1-norm of the errors at time $t = 1$ for the method of incomplete mesh adaptation with $L_{loop} = \max\{10, (M+1)/10\}$.

$\mathcal{H} \setminus M+1$	50	100	200	400
Density ρ				
10	9.37e-3	3.66e-3	1.74e-3	9.42e-4
20	7.13e-3	2.48e-3	1.08e-3	5.94e-4
Velocity u				
10	1.24e-2	4.37e-3	2.04e-3	9.73e-4
20	1.07e-2	3.37e-3	1.33e-3	6.06e-4
Internal energy ϵ				
10	2.04e-2	7.71e-3	3.80e-3	2.30e-3
20	1.52e-2	5.37e-3	2.42e-2	1.72e-3

Acknowledgments. The work was performed at the Los Alamos National Laboratory operated by the University of California for the US Department of Energy under contract W-7405-ENG-36. The authors acknowledge the partial support of the DOE/ASCR Program in the Applied Mathematical Sciences. The authors thank Mikhail Shashkov for valuable comments.

APPENDIX

Here, we shall motivate briefly the use of metric-based mesh adaptation in ALE simulations. Under certain assumptions, the following statements can be proved. First, the leading term in the total error is independent of $\mathcal{L}^n$. Therefore, an approximate solution to (6) can be found using only $\bar{\mathbf{u}}^n$ and $\mathbf{x}^n$. Second, an approximate solution to (6) is a $\mathcal{M}$-quasi-uniform mesh where metric $\mathcal{M}$ is induced by the first derivative of u.

Our assumptions are as follows. First, we assume solution regularity, i.e., the solution $u(x,t)$ has bounded second derivatives. Second, we assume exact data, i.e., the piecewise constant data $\bar{\mathbf{u}}^n$ representing $u(x,t)$ on $\mathbf{x}^n$ are exact. Third, let ξ be the Lagrangian coordinate, $x(\xi,t)$ be the transformation from Lagrangian to Cartesian coordinates such that $x(\xi,t^n) \in [x_i^n, x_{i+1}^n]$ when $\xi \in [\xi_i, \xi_{i+1}]$, and $e_{i+1/2}^n(x(\xi,t^n),t^n) \equiv u(x(\xi,t^n),t^n) - \bar{u}_{i+1/2}^n$ be the error function. We shall assume that the operator $\mathcal{L}^n$ is such that

$$|e_{i+1/2}^{n+1} - e_{i+1/2}^n| \leqslant C_{\mathcal{L}}(h_{i+1/2}^n + \Delta t^n)^2 \qquad \forall \xi \in [\xi_i, \xi_{i+1}]. \tag{18}$$

This estimate has been proven in[11] for the donor-type method applied to the 1D viscous Burgers's equation and for the predictor-corrector method applied to the system of 1D gas dynamics equations.

Let $E(u,t^n,\mathbf{x}^n)$ denote the L_1-norm of the error on mesh $\mathbf{x}^n$:

$$E(u,t^n,\mathbf{x}^n) = \sum_{i=0}^{M} \int_{x_i^n}^{x_{i+1}^n} |u(x,t^n) - \bar{u}([x_i^n, x_{i+1}^n], t^n)| dx.$$

For the function $u(x)$ with only one argument, we shall use the notation

$$E(u, \mathbf{x}) = \sum_{i=0}^{M} \int_{x_i}^{x_{i+1}} |u(x) - \bar{u}([x_i, x_{i+1}])| dx.$$

Theorem 1.[12] *Under assumptions of solution regularity, exact data, and conditions* **(C1)**, **(C2)**, *(18), the leading term of the error in (6) depends only on* $E(u, t^n, \tilde{\mathbf{x}}^n)$*:*

$$\|u(x, t^{n+1}) - \mathcal{L}^n(\overline{\tilde{\mathbf{u}}}^n)\|_{L_1([a,b])} = E(u, t^n, \tilde{\mathbf{x}}^n) + O((h + \Delta t^n)^2)|b - a|. \qquad (19)$$

The theorem allows us to replace the complicated problem (6) by a simpler problem: Find $\tilde{\mathbf{x}}^n_{opt}$ such that

$$\tilde{\mathbf{x}}^n_{opt} = \arg \min_{\tilde{x}^n_1, \ldots, \tilde{x}^n_M} E(u, t^n, \mathbf{x}^n). \qquad (20)$$

Now we turn to the approximate solution of problem (20) which provides the same error reduction for the piecewise constant interpolation as the optimal mesh $\tilde{\mathbf{x}}^n_{opt}$. Our second result states that a mesh uniform in $u'(x)$-metric is the approximate solution of the optimization problem (20).

Theorem 2.[12] *Let function* $u(x) \in C^2([a, b])$ *and* $u'(x) > 0$ *define the metric* $\mathcal{M}$ *on* $[a, b]$*. Furthermore, let mesh* $\tilde{\mathbf{x}}$ *given by (1) be* $\mathcal{M}$*-uniform,* $\tilde{h}_{\mathcal{M},i+1/2} = C_{\mathcal{M}}$*. Then there exists an integer* $M_0 > 0$ *and constant* C *independent of* u *and* h *such that for all* $M \geqslant M_0$

$$E(u, \tilde{\mathbf{x}}) \leqslant C E(u, \tilde{\mathbf{x}}_{opt}), \quad E(u, \tilde{\mathbf{x}}_{opt}) = \min_{x_1, \ldots, x_M} E(u, \mathbf{x}). \qquad (21)$$

References

[1] B.N. Azarenok, and S.A. Ivanenko. Application of adaptive grids in numerical analysis of time-dependent problems in gas dynamics. *Comput. Math. Math. Physics*, 40(9):1330–1349, 2000.

[2] G. Beckett, J. A. Mackenzie, A. Ramage, and D. M. Sloan. Computational solution of two-dimensional unsteady PDEs using moving mesh methods. *J. Comput. Phys.*, 182:478–495, 2002.

[3] H. Blum, S. Lisky, R. Rannacher. A domain splitting algorithm for parabolic problems. *Computing*, 49:11–23, 1992.

[4] J.U. Brackbill, and J.S. Saltzman. Adaptive zoning for singular problems in two dimensions. *J. Comput. Phys.*, 46:342–368, 1982.

[5] W. Cao, W. Huang, and R. D. Russell. An error indicator monitor function for r-adaptive finite-element method. *J. Comput. Phys.*, 170:871–892, 2001.

[6] E. Dorfi and L. Drury. Simple adaptive grids for 1-D initial value problems. *J. Comput. Phys.*, 69:175–195, 1987.

[7] A.S. Dvinsky. Adaptive Grid Generation from Harmonic Maps on Riemannian Manifolds. *J. Comput. Phys.*, 95:450–476, 1991.

[8] C.W. Hirt, A.A. Amsden, and J.L. Cook. An arbitrary Lagrangian-Eulerian computing method for all flow speeds. *J. Comp. Phys.*, 14:227–253, 1974.

[9] P. Knupp, L.G. Margolin, and M. Shashkov. Reference Jacobian optimization-based rezone strategies for arbitrary Lagrangian Eulerian methods. *J. Comp. Phys.*, 176:93–128, 2002.

[10] M. Kucharik, M. Shashkov, and B. Wendroff. An efficient linearity-and-bound-preserving remapping methods. *J. Comput. Phys.*, 188:462–471, 2003.

[11] K. Lipnikov and M. Shashkov. The error-minimization-based rezone strategy for arbitrary Lagrangian-Eulerian methods. *Numer. Meth. PDEs*, 22(3):617–637, 2006.

[12] K. Lipnikov and Yu. Vassilevski. Metric-based control of mesh adaptation in arbitrary Lagrangian Eulerian simulations. *Los Alamos Report LAUR-06-4765*, 2006.

[13] H. Tang, and T. Tang, Adaptive Mesh methods for one- and two-dimensional hyperbolic conservation laws. *SIAM J. Numer. Anal.*, 41:487–515, 2003.